Dynamic modulation of spatially structured polarization fields for real-time control of ultrafast laser-material interactions

Y. Jin,[1] O. J. Allegre,[1,*] W. Perrie,[1] K. Abrams,[2] J. Ouyang,[1] E. Fearon,[1] S. P. Edwardson,[1] and G. Dearden[1]

[1]*Laser Group, School of Engineering, University of Liverpool, L69 3GQ, UK*
[2]*Nanoinvestigation Centre at Liverpool, University of Liverpool, L69 3GQ, UK*
[*]*oallegre@liv.ac.uk*

Abstract: The polarization state of an ultrafast laser is dynamically controlled using two Spatial Light Modulators and additional waveplates. Consequently, four states of polarization, linear horizontal and vertical, radial and azimuthal, all with a ring intensity distribution, were dynamically switched at a frequency ν = 12.5Hz while synchronized with a motion control system. This technique, demonstrated here for the first time, enables a remarkable level of real-time control of the properties of light waves and applied to real-time surface patterning, shows that highly controlled nanostructuring is possible. Laser ablation of Induced Periodic Surface Structures is used to directly verify the state of polarization at the focal plane.

OCIS codes: (140.7090) Ultrafast lasers; (140.3390) Laser materials processing; (230.6120) Spatial light modulators; (140.3300) Laser beam shaping; (080.4865) Optical vortices; (260.5430) Polarization.

References and links

1. G. R. Fowles, *Introduction to Modern Optics* (Holt, Rinehart and Winston, Inc., New York, 1975), Chap. 2.
2. H. Kleinpoppen, *Constituents of Matter, Atoms, Molecules, Nuclei and Particles*, p142, Ed. Bergmann/Schaefer, Copyright Walter de Gruyer, Berlin, New York (1997), Berlin, Germany.
3. J. M. Guay, A. Villafranca, F. Baset, K. Popov, L. Ramunno, and V. R. Bhardwaj, "Polarization-dependent femtosecond laser ablation of poly-methyl methacrylate," New J. Phys. **14**(8), 085010 (2012).
4. R. W. Boyd, *Nonlinear Optics* (Academic press, Burlington MA, Elsevier, 2008), Chap. 4.
5. A. Braun, G. Korn, X. Liu, D. Du, J. Squier, and G. Mourou, "Self-channeling of high-peak-power femtosecond laser pulses in air," Opt. Lett. **20**(1), 73–75 (1995).
6. N. A. Panov, V. A. Makarov, V. Y. Fedorov, and O. G. Kosareva, "Filamentation of arbitrary polarized femtosecond laser pulses in case of high-order Kerr effect," Opt. Lett. **38**(4), 537–539 (2013).
7. L. Ye, Laser Group, School of Engineering, University of Liverpool, L69 3GQ, UK, W. Perrie, O. Allegre, Y. Jin, Z. Kuang, P. Scully, E. Fearon, D. Eckford, S. Edwardson, and G. Dearden are preparing a manuscript to be called "NUV femtosecond laser inscription of volume Bragg gratings in poly (methyl) methacrylate with linear and circular polarizations".
8. R. A. Fox, R. M. Kogan, and E. J. Robinson, "Laser Triple-Quantum Photoionization of Cesium," Phys. Rev. Lett. **26**(23), 1416–1417 (1971).
9. R. M. Kogan, R. A. Fox, G. T. Burnham, and E. J. Robinson, "Two-photon ionization of cesium," Bull. Am. Phys. Soc. **16**, 1411 (1971).
10. H. S. Carman and R. N. Compton, "High-order multiphoton ionization photoelectron spectroscopy of nitric oxide," J. Chem. Phys. **90**(3), 1307 (1989).
11. D. D. Venable and R. B. Kay, "Polarization effects in four-photon conductivity in quartz," Appl. Phys. Lett. **27**(1), 48–49 (1975).
12. V. V. Temnov, K. Sokolowski-Tinten, P. Zhou, A. El-Khamhawy, and D. von der Linde, "Multiphoton Ionization in Dielectrics: Comparison of Circular and Linear Polarization," Phys. Rev. Lett. **97**(23), 237403 (2006).
13. H. R. Reiss, "Polarization Effects in High-Order Multiphoton Ionization," Phys. Rev. Lett. **29**(17), 1129–1131 (1972).

#196357 - $15.00 USD Received 26 Aug 2013; revised 2 Oct 2013; accepted 4 Oct 2013; published 16 Oct 2013

14. P. G. Kazansky, W. Yang, E. Bricchi, J. Bovatsek, A. Arai, Y. Shimotsuma, K. Miura, and K. Hirao, "Quill Writing with ultrashort light pulses in transparent materials," Appl. Phys. Lett. **90**(15), 151120 (2007).
15. Y. Shimotsuma, P. G. Kazansky, J. Qiu, and K. Hirao, "Self-Organized Nanogratings in Glass Irradiated by Ultrashort Light Pulses," Phys. Rev. Lett. **91**(24), 247405 (2003).
16. Z. Guosheng, P. M. Fauchet, and A. E. Siegman, "Growth of spontaneous periodic surface structures on solids during laser illumination," Phys. Rev. B **26**(10), 5366–5381 (1982).
17. Q. Z. Zhao, S. Malzer, and L. J. Wang, "Formation of subwavelength periodic structures on tungsten induced by ultrashort laser pulses," Opt. Lett. **32**(13), 1932–1934 (2007).
18. C. Hnatovsky, V. Shvedov, W. Krolikowski, and A. Rode, "Revealing local field structure of focused ultrashort pulses," Phys. Rev. Lett. **106**(12), 123901 (2011).
19. S. Nolte, C. Momma, G. Kamlage, A. Ostendorf, C. Fallnich, F. Von Alvensleben, and H. Welling, "Polarization effects in ultrashort-pulse laser drilling," Appl. Phys., A Mater. Sci. Process. **68**(5), 563–567 (1999).
20. C. Föhl, D. Breitling, and F. Dausinger, "Precise drilling of steel with ultrashort plused solid-state lasers," Proc. SPIE **5121**, 271–279 (2003).
21. S. Hahne, B. F. Johnston, and M. J. Withford, "Pulse-to-pulse polarization-switching method for high-repetition-rate lasers," Appl. Opt. **46**(6), 954–958 (2007).
22. O. J. Allegre, W. Perrie, K. Bauchert, D. Liu, S. P. Edwardson, G. Dearden, and K. G. Watkins, "Real-time control of polarisation in ultra-short-pulse laser micro-machining," Appl. Phys., A Mater. Sci. Process. **107**(2), 445–454 (2012).
23. M. Beresna, M. Gecevicius, P. G. Kazansky, and T. Gertus, "Radially polarized optical vortex converter created by femtosecond laser nanostructuring of glass," Appl. Phys. Lett. **98**(20), 201101 (2011).
24. M. R. Beversluis, L. Novotny, and S. J. Stranick, "Programmable vector point-spread function engineering," Opt. Express **14**(7), 2650–2656 (2006).
25. O. J. Allegre, Y. Jin, W. Perrie, J. Ouyang, E. Fearon, S. P. Edwardson, and G. Dearden, "Complete wavefront and polarization control for ultrashort-pulse laser microprocessing," Opt. Express **21**(18), 21198–21207 (2013).
26. S. Hasegawa and Y. Hayasaki, "Holographic femtosecond laser processing by use of a spatial light modulator," Proc. SPIE **6458**, 645815 (2007).
27. C. Mauclair, A. Mermillod-Blondin, N. Huot, E. Audouard, and R. Stoian, "Ultrafast laser writing of homogeneous longitudinal waveguides in glasses using dynamic wavefront correction," Opt. Express **16**(8), 5481–5492 (2008).
28. S. Hasegawa and Y. Hayasaki, "Polarization distribution control of parallel femtosecond pulses with spatial light modulators," Opt. Express **21**(11), 12987–12995 (2013).
29. J. Zhang, M. Gecevicius, M. Beresna, and P. G. Kazansky, "5D Data Storage by Ultrafast Laser Nanostructuring in Glass", in *Conference on Lasers and Electro-Optics*, Technical Digest (online) (Optical Society of America, 2013), paper CTh5D. *http://www.opticsinfobase.org/abstract.cfm?URI=CLEO_SI-2013-CTh5D.9*
30. P. Mannion, J. Magee, E. Coyne, and G. M. O'Connor, "Ablation thresholds in ultrafast laser micro-machining of common metals in air," Proc. SPIE **4876**, 470–478 (2003).
31. U. Klug, J. F. Dusing, T. Sato, K. Washio, and R. Kling, "Polarization converted laser beams for micromachining applications," Proc. SPIE **7590**, 759006, 759006-8 (2010).
32. K. Lou, S. X. Qian, X. L. Wang, Y. Li, B. Gu, C. Tu, and H. T. Wang, "Two-dimensional microstructures induced by femtosecond vector light fields on silicon," Opt. Express **20**(1), 120–127 (2012).

1. Introduction

Polarization is a critical parameter in the linear and non-linear interaction of laser radiation with matter. For example, simple Fresnel reflection from a dielectric interface near Brewster's angle [1], atomic absorption and emission of light in the presence of a magnetic field (Zeeman effect) [2] and ultrafast laser surface ablation [3] all show significant effects of incident polarization state. In [3], the observed asymmetric ablation geometries and nano-structures were related to the direction of linear polarization. Also, high intensity non-linear phenomena such as self-focusing [4], filamentation [5–7] and multi-photon ionization (MPI) in atoms [8, 9], molecules [10] and solids [11, 12] are all polarization sensitive. With MPI at low non-linear order $N \leq 4$, circular polarization couples more strongly than linear [8, 9] while at high $N \geq 6$ a significant reversal occurs, decisively demonstrated in the 6-photon MPI of fused silica and sapphire with near-infrared (NIR), 50fs laser pulses yielding ($\sigma_6^{lin}/\sigma_6^{circ}$) ~3.7 and ~7 respectively [12] in agreement with theoretical predictions [13]. These differences arise from quantum selection rules, applicable even in solids and related to conservation of angular momentum during the absorption process.

Femtosecond inscription inside dielectrics with linear polarization can lead to birefringent photonic components [14] and nano-scale periodic modulation of refractive index through interference between the laser field and the electric field of bulk electron plasma waves [15].

#196357 - $15.00 USD Received 26 Aug 2013; revised 2 Oct 2013; accepted 4 Oct 2013; published 16 Oct 2013

In addition, surface nanostructuring of metals and semi-conductors with ultrashort laser pulses near ablation threshold creates wavelength-scale laser induced periodic surface structures (LIPSS), perpendicular to the local electric field vector and thus highly polarization sensitive [16, 17]. Furthermore, static plane wave radial and azimuthal polarization states have been used for demonstrating precise, high numerical aperture (NA = 0.9) nanostructuring of glass which revealed clearly the polarization states while also showing the predicted z-component of the electric field [18].

In all these examples, the ability to control and manipulate the state of polarization of the incident beam is desirable as it allows better control of laser-material interactions. A number of methods have been developed for polarization control. These methods can be categorized as dynamic or static. Dynamic methods typically involve modifying the direction of a linear polarization with time. For example, by using continuously rotating waveplates during laser microprocessing, the quality of the produced structures can be greatly improved [19–21]. However, the mechanical rotation of optical components can be adversely affected by vibrations and prone to mechanical failure. An alternative dynamic method used low bandwidth real-time switching between two orthogonal linear polarization states with the aid of a liquid-crystal polarization rotator [22]. Static methods include for example the generation of spatially structured polarization fields such as radial or azimuthal. These can be produced with a birefringent plate [23] or a Spatial Light Modulator (SLM) [24, 25].

In addition to polarization, SLMs also allow arbitrary control of a laser beam wavefront, thus leading to arbitrary parallel surface patterning [26] and real-time 3D femtosecond inscription in dielectrics [27]. Recently, with the aid of two SLMs, thin film nanostructuring with two fixed orthogonal linear states of polarization was demonstrated, avoiding interference between adjacent spots [28]. In another important recent development, 5D, high NA femtosecond inscription of arbitrary directed birefringent structures was demonstrated by combining a SLM and special birefringent micro-structured waveplate [29]. Furthermore, our previous research [25] involved the generation of parallel beams with static radial and azimuthal polarizations for ultrafast laser microprocessing using two SLMs, although the dynamic capabilities of SLMs were not used in [25].

Dynamical switching of arbitrary polarization states opens up the possibility to further control the light field – material interactions in a highly desirable and flexible manner, however to the best of our knowledge this has not been demonstrated previously. This paper thus introduces dynamic control of spatially structured polarization fields in a picosecond-pulse laser microprocessing system, using two phase-only SLMs in series. As a proof of concept, the polarization was modulated at a speed of up to 12.5Hz, switching between four distinct states: linear horizontal and vertical, radial and azimuthal, whilst scanning the beam on the surface of a highly polished steel sample. The polarization modulation was analyzed through surface plasmon nanostructuring of LIPSS within the exposed regions of the samples. This approach clearly demonstrated that the desired polarization states were achieved with high fidelity and fully synchronized with laser pulse micro-positioning at the target surface. Symmetric surface patterns with multi-pulse exposure as well as results with beam scanning are presented, fully confirming the polarization switching and synchronization.

2. Experimental details

2.1 Experimental setup

A schematic of the experimental setup is shown in Fig. 1. The laser source is a Coherent Talisker with a pulse width of 10ps, a wavelength of 532nm (linewidth ~0.1nm), M^2 <1.3, average power of 8W, 200kHz maximum repetition rate and a horizontal linear polarization. The beam is expanded using a telescope (Jenoptic) with ×3 magnification. To modulate wavefront as well as polarization, two Hamamatsu X10468-04 LCOS-SLMs (Liquid-Crystal On Silicon Spatial Light Modulators) and a pair of zero-order waveplates are used (Fig. 1).

#196357 - $15.00 USD Received 26 Aug 2013; revised 2 Oct 2013; accepted 4 Oct 2013; published 16 Oct 2013

The SLMs (referred to as SLM1 and 2 in Fig. 1) are of the phase-only, reflection type and consist of a 16x12mm, 800x600 pixel array of horizontally oriented liquid-crystal phase retarders. SLM1 is used to control the wavefronts whereas SLM2, together with the waveplates, is used to control polarization.

After the SLMs, there is 4f optical system (Lens 1 and 2 in Fig. 1) which uses plano-convex lenses (f = 400mm) to re-image the surface of SLM2 (Fig. 1) to the 15mm input aperture of a scanning galvo (Nutfield). At the galvo output, the beam is focused with a flat field f-theta lens (f = 250mm). For processing experiments, samples are mounted on a precision 3-axis (x, y, z) motion control system (A3200 Ndrive system, Aerotech) allowing accurate positioning in the focal plane. The modulation of polarization is synchronized with the beam scanning motion on the sample thanks to a real-time control unit Aerotech Nmark SSam (Synchronized Scanning and motion) which runs within a Labview environment, driving the scanning galvo as well as synchronizing application of previously Computer-Generated phase Holograms (CGHs) to the SLMs.

Prior to processing the samples, the collimated beam is analyzed with a SPIRICON beam profiler and a polarizing filter located just before Lens 1 (see Fig. 1). The camera had no focusing lens.

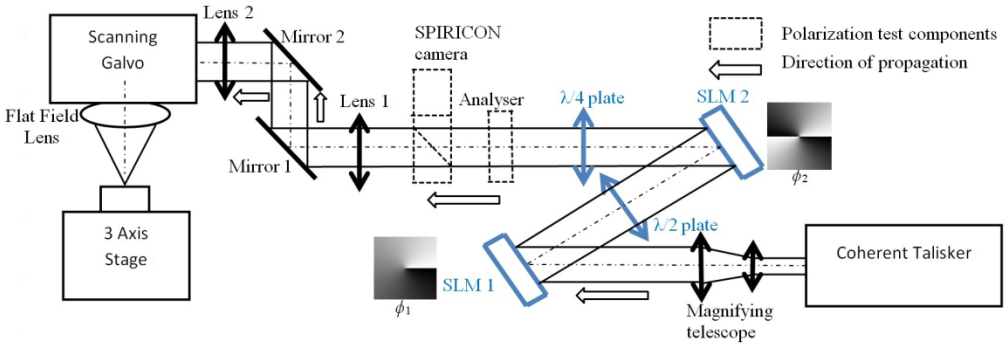

Fig. 1. Schematic showing how the SLMs together with the waveplates are used to control the wavefront and polarization of a picosecond-pulse laser microprocessing setup. The laser source provides a 532nm wavelength, 10ps pulse beam with a horizontal linear polarization, incident on SLM1. After SLM1, a half-waveplate tilts the polarization direction to + 45°, incident on SLM2. In this setup, SLM1 is used to control the wavefront whereas SLM2 is used to control the polarization. The "polarization test components" are removed when the microprocessing tests are carried out.

2.2 Optical configurations

The beams produced with the SLM-based setup can be expressed as a Jones vector noted $J(x,y)$, where x and y are the horizontal and vertical coordinates across the beam profiles. A full derivation using the optical properties of the setup [25] gives:

$$J(x,y) = e^{-i\frac{\pi}{2}} \times e^{i\phi_1(x,y)} \times e^{i\frac{\phi_2(x,y)}{2}} \times \begin{pmatrix} \sin\frac{\phi_2(x,y)}{2} \\ \cos\frac{\phi_2(x,y)}{2} \end{pmatrix} \quad (1)$$

where $\phi_1(x,y)$ and $\phi_2(x,y)$ are the relative phase delays, or CGHs, induced with the first and second SLM respectively (Fig. 1). Equation (1) shows that the wavefront and polarization can be controlled by adjusting $\phi_1(x,y)$ and $\phi_2(x,y)$ respectively, so that the resulting beams have the desired optical field structures. For the experiments, the SLMs were configured to produce four distinct optical field configurations: linearly polarized beams (horizontal or vertical) with a vortex wavefront (carrying an orbital angular momentum of l = 1), or radially and azimuthally polarized beams with a planar wavefront. The values $\phi_1(x,y)$ and $\phi_2(x,y)$ in each

#196357 - $15.00 USD Received 26 Aug 2013; revised 2 Oct 2013; accepted 4 Oct 2013; published 16 Oct 2013

case are summarized in Fig. 2. The (fixed) CGH applied to SLM1 (expressed as $\phi_1(x,y)$ in Fig. 2) created a vortex wavefront whereas the four CGHs sequentially applied to SLM2 (expressed as $\phi_2(x,y)$ in Fig. 2) modulated the polarization states. All these optical field configurations produce the same ring-shaped intensity distribution when focused with a low NA lens such as the one used in our experiment. Therefore the fluence at the sample surface is the same in each case. Importantly, the SLMs enable to dynamically control $\phi_1(x,y)$ and $\phi_2(x,y)$ so that the state of polarization can be modulated in real-time.

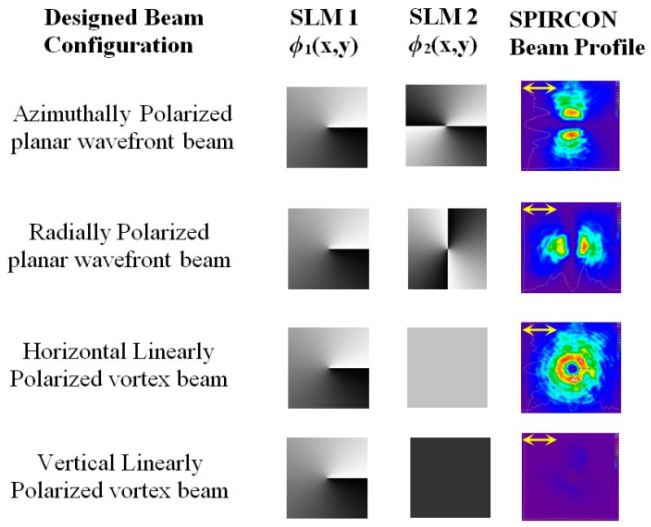

Fig. 2. Summary of the various beam configurations used for the experiments. $\phi_1(x,y)$ and $\phi_2(x,y)$ are adjusted to shape the beam wavefront and polarization respectively. The resulting collimated beams are analyzed with a horizontally-oriented polarizing filter and SPIRICON beam profiler, located just before Lens 1 (see Fig. 1). The (unfocused) beam profile observed in each configuration is shown in the right-hand column (the color-coded scale represents intensity in arbitrary units and the arrows represents the transmission axis of the analyzer). Note that the vertical linearly polarized beam is completely blocked by the analyzer.

2.3 Experimental procedure

For the experiments, the modulated laser beam is used to process the surface of a highly polished stainless steel sample, using a fluence near the ablation threshold of steel, which is ~0.16J/cm^2 [30]. This leads to the formation of wavelength-sized LIPSS, which develop orthogonally to the local electric field vectors of the beam [16, 17]. Therefore, by modulating the incident polarization field, we control the way LIPSS develop on the surface. The experiments consisted in laser processing the sample surface, whilst dynamically changing the polarization fields so as to produce the desired LIPSS patterns over large scales.

For all these tests, the laser output is attenuated to produce a pulse energy of 3μJ (fluence F ~0.2J/cm^2 at focal plane). Various processing geometries are used, where the sample is exposed to produce either sets of discrete laser spots or continuous scanned lines. In the former case each spot is exposed for 20ms whilst the beam remains static and in the latter case the beam is scanned at 2.5mm/s. In either case each region is exposed with an average pulse overlap of ~100pulses, with a pulse repetition rate of 5kHz. After laser exposure, the processed surfaces are imaged with an optical microscope and Scanning Electron Microscope (SEM).

#196357 - $15.00 USD Received 26 Aug 2013; revised 2 Oct 2013; accepted 4 Oct 2013; published 16 Oct 2013

3. Results and discussion

Thanks to its flexibility, the setup allows processing a wide range of geometries, where the desired state of polarization is applied within each region. A number of experimental configurations are demonstrated below.

3.1 Discrete patterns of laser spots with polarization control

As a first case study, the experimental setup was configured to produce a discrete pattern of laser spots, where the overall geometry was designed to represent four letters "LLEC" (Fig. 3, representing Lairdside Laser Engineering Centre), each with a distinct state of polarization. Thus, four sets of laser spots are sequentially produced so that each letter of the geometry has a different state of polarization. Each spot was imprinted with 100 pulses at 0.2J/cm^2 (see processing parameters in Section 2.3 above) and the overall exposure duration for the whole geometry was ~4s (52spots) corresponding to a polarization switching bandwidth of ~1Hz.

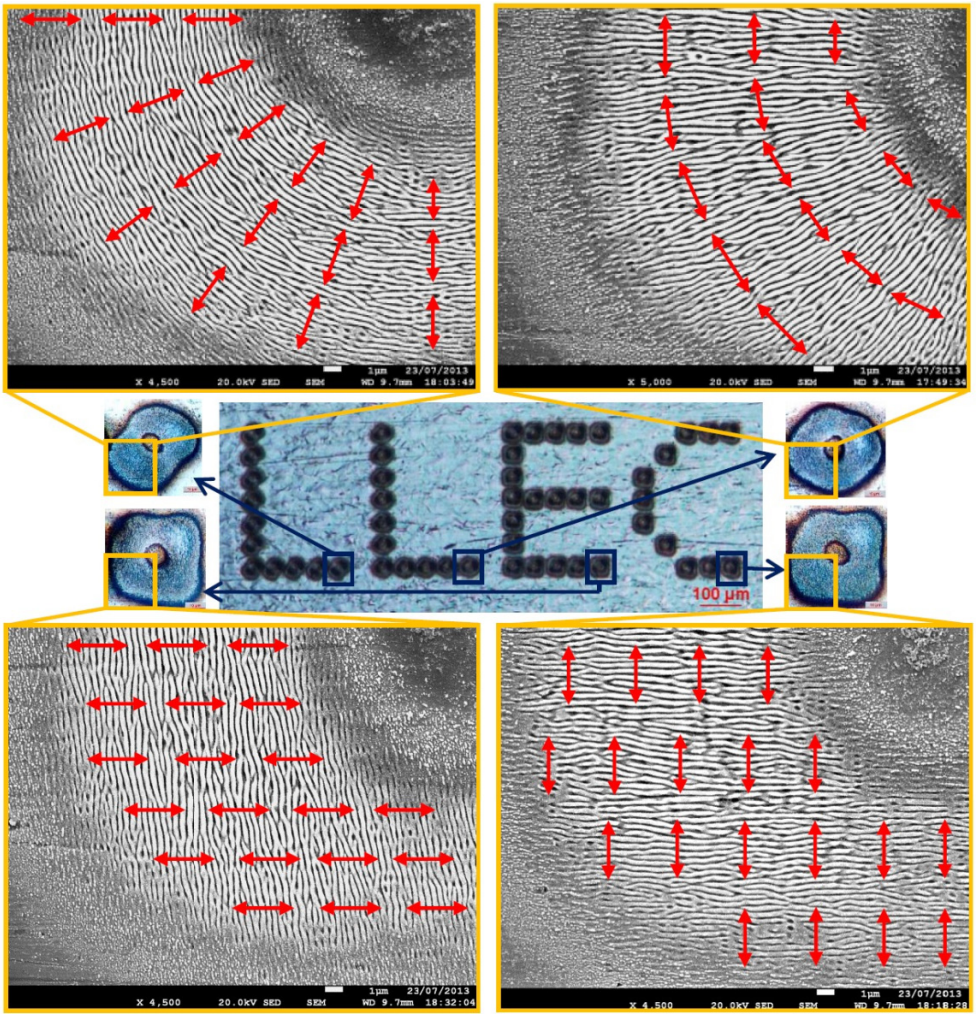

Fig. 3. (Centre) Optical micrographs showing the processed geometry, which is produced by marking four distinct sets of laser spots, each set using a different state of polarization. (Top and bottom) magnified regions of laser spots, imaged with an SEM. The ablation spots had been produced either with a radially (top-left inlay), azimuthally (top-right inlay), horizontally (bottom-left) and vertically (bottom-right) polarized beam. The red arrows represent the direction of local electric field vectors.

#196357 - $15.00 USD Received 26 Aug 2013; revised 2 Oct 2013; accepted 4 Oct 2013; published 16 Oct 2013

The bandwidth of polarization switching was calculated approximately from the time taken to micro-structure the overall pattern, allowing for the number of switching cycles during the procedure (with nearly the same number of spots in each letter).

After laser processing, a microscopic investigation of the produced geometry revealed the details of the laser spots (Fig. 3). As expected, each produced laser spot had a ring-shaped structure. The laser exposure had also led to the development of LIPSS within each spot. The geometry of LIPSS, imaged with an SEM in Fig. 3, is consistent with that expected when processing with a linear, radial or azimuthal state of polarization, in line with [16, 31, 32]. Note that the micro-machined spots do show some residual distortion in their shape due to the resolution limit of the SLMs, where the pixel size (~20μm) and discrete phase modulation induced some discontinuity in the produced wavefronts which affected the focal intensity distributions.

The polarization states are also easily visualized using low-angle side illumination shown in optical micrographs, Figs. 4(a) and 4(b) where two illumination sources (white light, unpolarized) at grazing incidence were used, located on either side of the sample along a single axis (red arrows in Fig. 4). Due to their diffractive properties, only the areas where LIPSS are perpendicular to the axis of illumination reflected the low-angle light, Fig. 4(a), while the other areas remain dark. Therefore, each microscope image shows the part of the geometry that reflected the illumination through diffraction on the LIPSS. Rotating the axis of illumination by 90° reveals the remainder of the geometry, Fig. 4(b). This confirmed that each set of laser spots (i. e. each letter of the geometry) has a distinct LIPSS pattern, hence the desired states of polarization have been successfully achieved and confirmed unambiguously from these diffractive patterns.

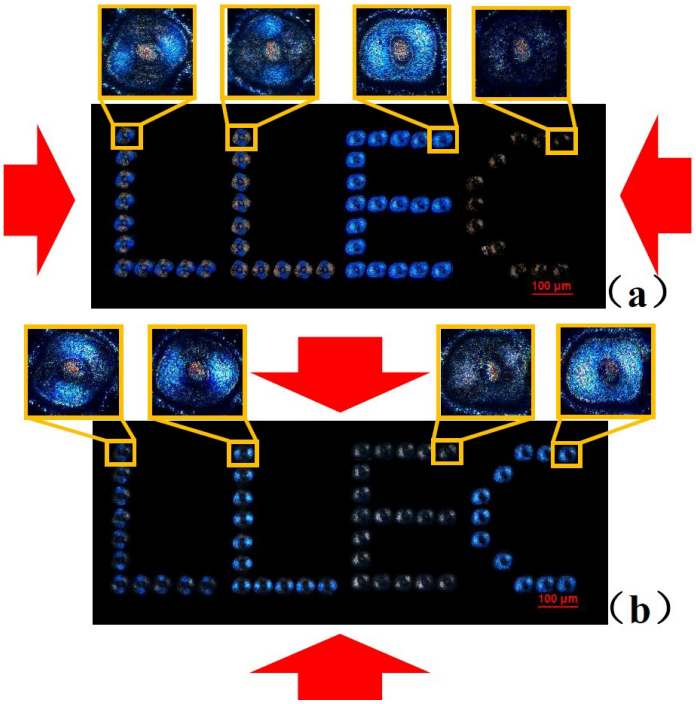

Fig. 4. Optical micrographs showing the processed geometry, imaged with side-illumination at grazing incidence. The illumination source was a white light, unpolarized source from a tungsten lamp coupled through a flexible optical fiber. The red arrows show the axis of illumination, which is horizontal in (a) and vertical in (b). Thanks to the diffractive properties of LIPSS, only the areas that had been exposed with polarization vectors parallel to this axis reflect the low angle illumination through the microscope. The other areas remain dark.

#196357 - $15.00 USD Received 26 Aug 2013; revised 2 Oct 2013; accepted 4 Oct 2013; published 16 Oct 2013

3.2 Arrays of laser spots with dynamic polarization control

The states of polarization can be easily modulated in real-time during processing. The experimental setup was configured to produce discrete patterns of laser spots arranged in a square array, each with the desired LIPSS orientation. As before, each spot is produced with 100 pulses at 0.2J/cm^2, as described in Section 2.3 above.

Figure 5 shows an array of laser spots produced using two orthogonal states of polarization, linear horizontal and linear vertical (and with a vortex wavefront, as described in Section 2.2). The polarization direction is set to horizontal to imprint a first set of four laser spots at the chosen locations within the geometry. The polarization is then flipped synchronously to the vertical direction and a second set of four laser spots is imprinted. This process is repeated several times to produce the overall laser spots array (i.e. 36 sets of four laser spots). The resulting pattern, (Fig. 5) is beautifully symmetric with alternating arrays of laser spots with orthogonal LIPSS orientations. As hardware and software timing delays had not been optimized at this stage, the time required to produce the whole array (144 laser spots) was ~22s. The average time to micro-machine each set of four spots was therefore 22/36 = 0.61s and the effective polarization switching bandwidth was ν = 1.6Hz.

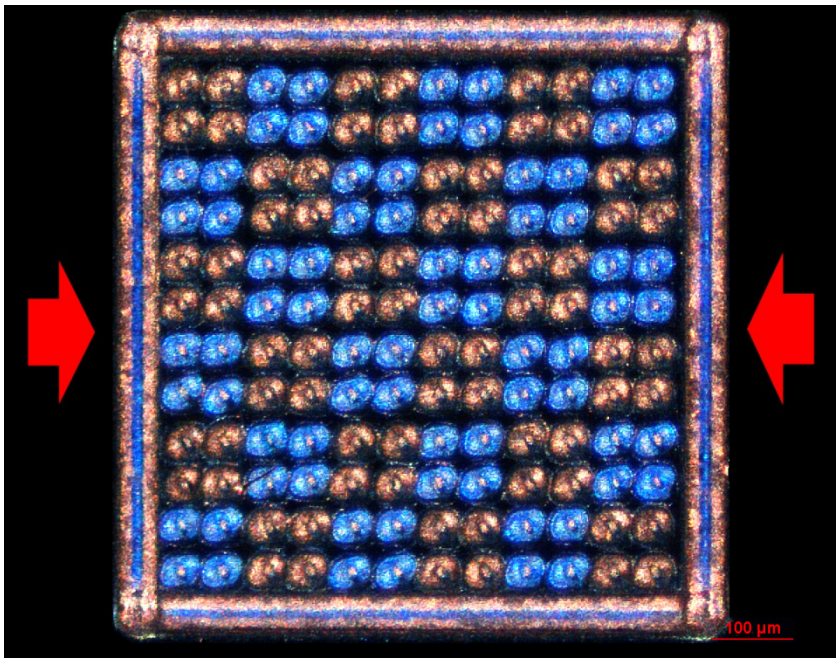

Fig. 5. Optical micrograph showing the produced array of laser spots, imaged with side-illumination at grazing incidence (red arrows). Thanks to the diffractive properties of LIPSS, only the areas that had been exposed with polarization vectors parallel to the red arrows reflect the low angle illumination through the microscope. The other areas remain dark. This confirmed that the expected state of polarization had been applied in each region of the processed area.

By optimizing all timing delays in software and hardware, dynamic polarization modulation was achieved by switching the 4 polarization states sequentially in real-time thus generating a new array on the surface where every spot in turn imprinted a different LIPSS nano-structure, Fig. 6. The time taken to micro-machine the 144 spots was ~11.5s hence the average time period between each spot was 11.5/144 = 0.08s and the polarization switching bandwidth was ν = 12.5Hz. This experiment confirmed that dynamic control of spatially structured polarization fields has been completely achieved. The high degree of symmetry

#196357 - $15.00 USD Received 26 Aug 2013; revised 2 Oct 2013; accepted 4 Oct 2013; published 16 Oct 2013

throughout the pattern supports robust, effective polarization switching at this frequency of 12.5Hz.

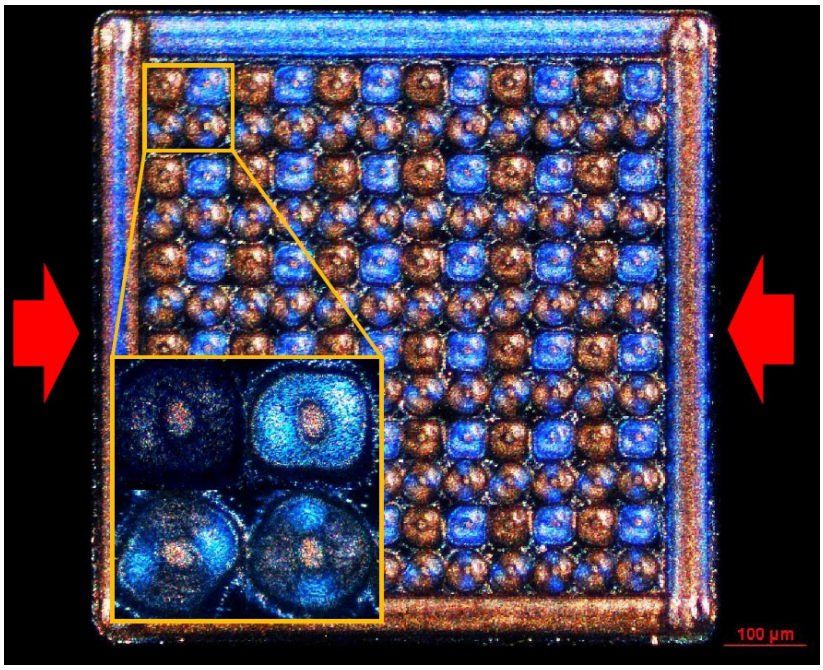

Fig. 6. Optical micrograph showing a laser spot array, imaged with side-illumination at grazing incidence (red arrows). Thanks to the diffractive properties of LIPSS, only the areas that had been exposed with polarization vectors parallel to the red arrows reflect the low angle illumination through the microscope. The array had been processed by sequentially marking sets of four laser spots, each with a distinct state of polarization. The bottom-left inlay shows one such set of laser spots.

3.3 Continuous linear scanning with dynamic polarization control

Finally, we show that complex two dimensional patterns of LIPSS can be produced using linear scanning with dynamic control of polarization. The setup was configured to scan along a raster pattern, where polarization was sequentially changed during scanning. As before, the state of polarization was synchronized with the beam scanning motion so as to produce the desired pattern of LIPSS in each region of the scanned geometry. The processing parameters are described in Section 2.3 above. Figure 7 shows optical micrographs of the produced figures and confirms once more that synchronization is complete. The microscopic analysis confirmed that the expected, complex LIPSS patterns had been produced in each region with polarizations switched synchronously again at $\nu = 12.5$Hz.

#196357 - $15.00 USD Received 26 Aug 2013; revised 2 Oct 2013; accepted 4 Oct 2013; published 16 Oct 2013

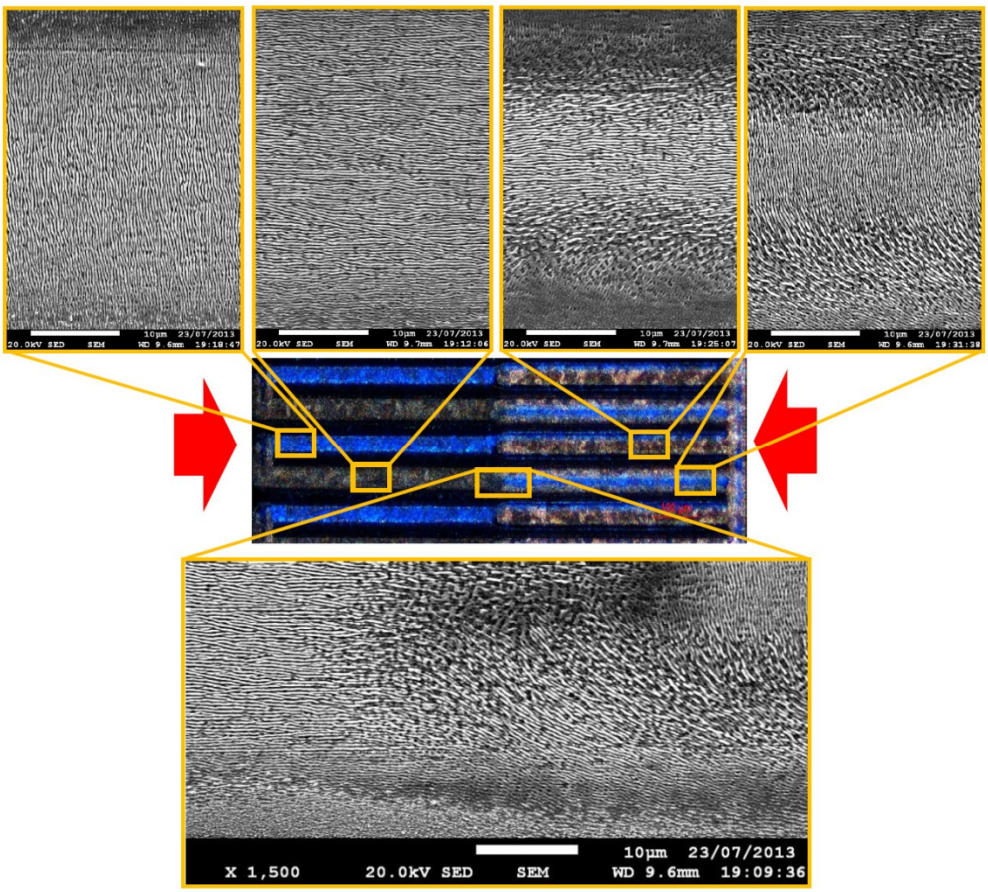

Fig. 7. (Centre) Optical micrograph showing the processed area, imaged with side-illumination at grazing incidence (red arrows). Four states of polarization, linear horizontal and vertical, radial and azimuthal were sequentially produced to process each region within the scanning path. The magnified inlays (top and bottom) show SEM images of the complex patterns of LIPSS imprinted in each region.

5. Conclusions

Real-time modulation of spatially structured polarization fields has been demonstrated, using two phase-only SLMs combined with two waveplates and addressed dynamically to produce four distinct polarization states, sequentially swapped at a frequency of up to ν = 12.5 Hz. Radial and azimuthal as well as orthogonal linear polarization states were generated with high fidelity, all with a ring intensity distribution.

By synchronizing the SLMs with a Galvo micro-positioning system, complex, real-time surface nanostructuring was demonstrated on a polished metal sample. Chess board type spot arrays (12 x 12) were micro-machined in a time τ = 11.5 seconds, confirming polarization switching at up to a frequency ν = 12.5Hz as well as linear scanning with real-time synchronized polarization modulation. Arrays of desired polarization states and associated vector fields were confirmed unambiguously by observing LIPSS which are generated orthogonal to the local electric field vector components and further elucidated by the directional light diffraction from the LIPSS.

Dynamic, real-time technique for fast polarization modulation with SLM's is demonstrated here for the first time and has great potential for industrial applications in both

#196357 - $15.00 USD Received 26 Aug 2013; revised 2 Oct 2013; accepted 4 Oct 2013; published 16 Oct 2013

surface and volume micro and nano-structuring. Potential applications may, for example include complex security marking and the creation of photonic components (using high and low NA) via femtosecond inscription, including data storage. In terms of research potential, polarization dependent spectroscopies might well benefit from fast differential polarization measurements at these bandwidths. Efforts to increase the effective polarization switching bandwidth are now in progress.

Acknowledgments

The authors gratefully acknowledge the support of the EPSRC as well as the help of Prof. Miles Padgett who provided the SLM control software used in this research and of Jack Bennett at Hamamatsu UK for the loan of SLMs.

#196357 - $15.00 USD Received 26 Aug 2013; revised 2 Oct 2013; accepted 4 Oct 2013; published 16 Oct 2013